Bulgarian Chemical Communications, Volume 54, Issue 2 (pp.134-140) 2022 DOI: 10.34049/bcc.54.2.5454

MHD Eyring-Powell nanofluid flow in a channel with oscillatory pressure gradient: A note

P. B. Kumar, S. Srinivas*

Department of Mathematics, VIT-AP University, Inavolu – 522 237, Near Vijayawada, Andhra Pradesh, India.

Received: November 01, 2021; Revised: March 03, 2022

This article describes the MHD Eyring-Powell nanofluid flow with oscillatory pressure gradient in an impermeable vertical channel. Here, blood and various shapes of alumina (Al_2O_3) are taken as non-Newtonian base-fluid and nanoparticles, respectively. Maxwell Garnett and Brinkman models are used to calculate the thermophysical properties of the nanofluid. Governing flow equations are simplified and the resulting system of non-linear differential equations is solved by Shooting technique along with the Runge-Kutta fourth-order method The effects of arising parameters on the flow variables have been studied in detail and numerical results are depicted graphically.Numerical results for the Nusselt number are presented in tabular form for different shapes of nanoparticles.

Keywords: Eyring-Powell nanofluid, Pulsating flow, Hartmann number, Grashof number.

INTRODUCTION

Nanoparticles are used as drug delivery carriers which are usually less than 100 nm and contain various biodegradable elements such as natural/synthetic polymers/metals [1]. Choi and Eastman [2] noticed that the nanofluids enhance the thermal conductivity, as well as the heat transfer in base fluids. Since then, studies pertaining to nanofluids have attracted the attention of many researchers (see [3-8]) due to the rapid development of nanotechnology in engineering and sciences.

Oscillatory flow is a periodic flow oscillating around a non-zero mean value. In recent times, the studies pertaining to pulsating flows gain a great deal of research attention because of their applications in biological areas such as human circulatory, respiratory and vascular systems and in engineering areas such as fuel injection into or exhaust from internal combustion engines, thermo-acoustic coolers and MEMS microfluidic engineering applications [9-12]. Abou-zeid *et al.* [13] examined the heat and mass transfer of a pulsating flow of a non-Newtonian fluid through permeable parallel plates saturated with porous medium. Recently, Jafarzadeh *et al.* [14] simulated the unsteady pulsatile blood flow distribution of nanoparticles loaded with the drug in the artery by taking blood as non-Newtonian in character. Very recently, Kumar and Srinivas [15] numerically studied the combined effects of slip-velocity and Joule's heating on the MHD pulsating flow of Eyring–Powell nanofluid through a vertical porous channel.

Several mathematical models have been developed to understand the flow behaviour pertaining to the oscillatory flows in different flow configurations (see Refs. [16-21] and several references therein).

A study related to MHD oscillatory flow of an Eyring-Powell nanofluid through the vertical channel considering the shape factor has not yet been reported, to the best of authors' knowledge. So, the main aim of the present study is to examine the flow of an Eyring-Powell nanofluid with oscillating pressure gradient accounting for the magnetic field, Joule's heating and thermal radiation. In this investigation, blood is taken as the base fluid and Al_2O_3 is considered as nanoparticle. Effects of important parameters on the momentum and heat transfer characteristics were analysed with the help of computer illustrations. Results for the rate of heat transfer are presented for four different shapes of nanoparticles. This paper is organised as follows: mathematical formulation, results along with discussion and conclusions.

MATHEMATICAL FORMULATION

As shown in Fig. 1, the flow of the fluid is only in the $x-$ direction, and we have taken the oscillatory flow of the Eyring-Powell fluid in the vertical channel. The fluid is electrically conducting due to the applied magnetic field B_0. The polarization is negligible because of lower magnitude of external magnetic field, hence there will be no internal electric field. The temperature on the left wall of the channel is T_0 while the uniform temperature T_1 is considered on the right wall. The impact of thermal radiation in the equation of energy, is taken into

---

* To whom all correspondence should be sent:
E-mail: srinusuripeddi@hotmail.com

account. The momentum and energy equations considering the Boussinesq approximation for the flow are [15, 19, 22]:

$$\frac{\partial \hat{u}}{\partial \hat{t}} = -\frac{1}{\rho_{nf}}\frac{\partial \hat{p}}{\partial \hat{x}} + \frac{\mu_{nf}}{\rho_{nf}}\left(1+\frac{1}{\gamma C \mu_{nf}}\right)\frac{\partial^2 \hat{u}}{\partial \hat{y}^2} + g\beta_{nf}\left(\hat{T}-T_0\right) - \frac{\sigma_{nf}B_0^2}{\rho_{nf}}\hat{u} \tag{1}$$

$$\frac{\partial \hat{T}}{\partial \hat{t}} = \frac{\kappa_{nf}}{\left(\rho c_p\right)_{nf}}\frac{\partial^2 \hat{T}}{\partial \hat{y}^2} + \frac{\mu_{nf}}{\left(\rho c_p\right)_{nf}}\left(1+\frac{1}{\gamma C \mu_{nf}}\right)\left(\frac{\partial \hat{u}}{\partial \hat{y}}\right)^2 + \frac{Q_0}{\left(\rho c_p\right)_{nf}}\left(\hat{T}-T_0\right) + \frac{\sigma_{nf}}{\left(\rho c_p\right)_{nf}}B_0^2\hat{u}^2 - \frac{1}{\left(\rho c_p\right)_{nf}}\frac{\partial q_r}{\partial \hat{y}} \tag{2}$$

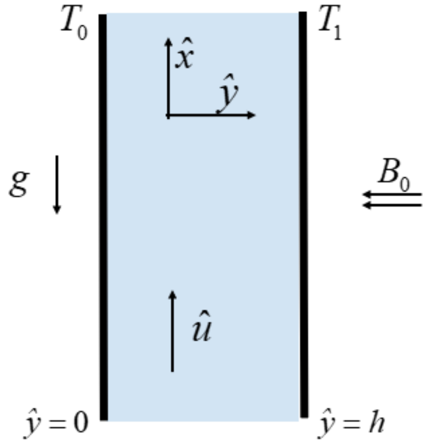

Figure 1. Physical sketch of the flow.

The velocity and temperature fields are subjected to the following conditions:

$$\text{on left wall: } \hat{u}=0 \text{ and } \hat{T}=T_0\text{; on right wall: } \hat{u}=0 \text{ and } \hat{T}=T_1. \tag{3}$$

Flow of the fluid in the channel is influenced by an oscillatory pressure gradient [18]:

$$-\frac{1}{\rho_f}\frac{\partial \hat{p}}{\partial \hat{x}} = A\left[1+\varepsilon e^{(\hat{t}\,\omega)\,i}\right]; \quad \varepsilon \ll 1 \tag{4}$$

where, the subscript *f* indicates the base fluid; *nf* indicates the nanofluid; ^ indicates the dimensional variable; μ_{nf} the dynamic viscosity; $A\rho_f$, amplitude of the oscillating pressure gradient; γ and C are the Eyring-Powell fluid parameters; $\hat{u}$, $\hat{v}$ are the components of velocity along x, y axes; $\hat{p}$, the dimensional pressure; ρ_{nf}, the density; g, the gravitational force; β_{nf} denotes the thermal expansion coefficient; $\hat{T}$ represents the dimensional temperature of the fluid; σ_{nf} the electrical conductivity; B_0, the magnetic field strength; $\hat{t}$, the dimensional time; κ_{nf}, the thermal conductivity; $\left(\rho c_p\right)_{nf}$, the specific heat and Q_0 indicates the heat source (or sink).

The radiative heat flux, q_r, is simplified according to the Rosseland approximation as:

$$q_r = \frac{-4}{3}\left(\frac{\partial \hat{T}^4}{\partial \hat{y}}\right)\frac{\hat{\sigma}}{\hat{k}} \tag{5}$$

where, $\hat{\sigma}$ represents the Stefan–Boltzmann constant, the coefficient of Rosseland mean absorption represented by $\hat{k}$ and $\hat{T}^4 \cong 4T_1^3\hat{T} - 3T_1^4$ [15].

Presenting the non-dimensional variables to transform the flow equations (1) - (5) into the non-dimensional form [7, 23]:

$$u = \hat{u}\omega / A;\ p = \hat{p} / A\rho_f h;\ t = \hat{t}\omega;\ \theta = \left(\hat{T}-T_0\right)/\left(T_1-T_0\right);\ x = \hat{x}/h;\ y = \hat{y}/h \tag{6}$$

where, ω is the angular frequency, u is the velocity and θ is the temperature in dimensionless form.

The nanofluid's physical characteristics are represented as [3, 15, 22, 24]:

$$\left.\begin{array}{c} A_1 = \dfrac{1}{(1-\phi)^{2.5}} = \dfrac{\mu_{nf}}{\mu_f}; \quad A_2 = (1-\phi)+\phi\left(\dfrac{\rho_n}{\rho_f}\right) = \dfrac{\rho_{nf}}{\rho_f}; \\ A_3 = (1-\phi)+\phi\left(\dfrac{\left(\rho c_p\right)_n}{\left(\rho c_p\right)_f}\right) = \dfrac{\left(\rho c_p\right)_{nf}}{\left(\rho c_p\right)_f}; \\ A_4 = \dfrac{\kappa_n + (m-1)\kappa_f - (m-1)\phi\left(\kappa_f - \kappa_n\right)}{\kappa_n + (m-1)\kappa_f + \phi\left(\kappa_f - \kappa_n\right)} = \dfrac{\kappa_{nf}}{\kappa_f}; \\ A_5 = 1 + \dfrac{3\left(\left(\sigma_n/\sigma_f\right)-1\right)\phi}{\left(\left(\sigma_n/\sigma_f\right)+2\right)-\left(\left(\sigma_n/\sigma_f\right)-1\right)\phi} = \dfrac{\sigma_{nf}}{\sigma_f}; \\ A_6 = (1-\phi)+\phi\left(\left(\rho\beta\right)_n/\left(\rho\beta\right)_f\right) = \dfrac{\left(\rho\beta\right)_{nf}}{\left(\rho\beta\right)_f} \end{array}\right\} \tag{7}$$

where, ϕ is the nanoparticle volume fraction, m is the shape factor, the subscript n is the nanoparticle.

Transforming the Eqs. (1) – (2) by using Eqs. (5) – (7) we get:

$$-\frac{\partial p}{\partial x} = 1 + \varepsilon e^{it} \tag{8}$$

$$H^2\frac{\partial u}{\partial t}=-\frac{H^2}{A_2}\frac{\partial p}{\partial x}+\left(\frac{A_1}{A_2}\right)\left(1+\frac{k_1}{A_1}\right)\frac{\partial^2 u}{\partial y^2}+\left(\frac{A_6}{A_2}\right)(Gr)\theta-\left(\frac{A_5}{A_2}\right)M^2u \tag{9}$$

$$H^2\frac{\partial\theta}{\partial t}=\left(\frac{A_4}{A_3}\frac{1}{\Pr}+\frac{4}{3A_3}\frac{Rd}{\Pr}\right)\frac{\partial^2\theta}{\partial y^2}+\left(\frac{A_1}{A_3}\right)\left(1+\frac{k_1}{A_1}\right)Ec\left(\frac{\partial u}{\partial y}\right)^2+\left(\frac{A_5}{A_3}\right)Ec\left(M^2\right)u^2+\left(\frac{Q}{A_3}\right)\theta \tag{10}$$

The transformed conditions are as follows:

$$\text{at}\, y=0: u=0 \text{ and } \theta=0; \qquad \text{at}\, y=1: u=0 \text{ and } \theta=1 \tag{11}$$

where, $H=h\sqrt{\omega/\upsilon_f}$ (frequency parameter), $\Pr=\upsilon_f\left(\rho c_p\right)_f/\kappa_f$ (Prandtl number), $M=B_0h\sqrt{\sigma_f/\mu_f}$ (Hartmann number), $Q=Q_0h^2/\left[\upsilon_f\left(\rho c_p\right)_f\right]$ (heat source/sink parameter), $Ec=A^2/\left[\omega^2(c_p)_f\left(T_1-T_0\right)\right]$ (Eckert number), $k_1=1/\left(\gamma C\mu_f\right)$ (non-Newtonian parameter), $Gr=g\beta_f\left(T_1-T_0\right)\omega h^2/\left(A\upsilon_f\right)$ (Grashof number), $\upsilon_f=\mu_f/\rho_f$ (kinematic viscosity) and $Rd=\left(4\hat{\sigma}T_1^3\right)/\left(\kappa\hat{k}\right)$ (radiation parameter).

A perturbative solution has been assumed to derive the solution for the transformed equations in the form [22, 25]:

$$u(y,t)=u_0(y)+\varepsilon u_1(y)e^{it};\quad \theta(y,t)=\theta_0(y)+\varepsilon\theta_1(y)e^{it}. \tag{12}$$

Here, u_0 and θ_0 are the zeroth-order terms; u_1 and θ_1 are first-order terms of the perturbative solution of the velocity and temperature distributions, respectively.

Incorporating Eq. (12) in Eqs. (8) – (11) and on equating the coefficients of different powers of ε we get:

$$B_1u_0''+B_3u_0+B_2\theta_0+B_4=0 \tag{13}$$

$$B_1u_1''+B_5u_1+B_2\theta_1+B_4=0 \tag{14}$$

$$B_6\theta_0''+B_7\left(u_0'\right)^2+B_8\left(u_0\right)^2+B_{10}\theta_0=0 \tag{15}$$

$$B_6\theta_1''+\left(B_9+B_{10}\right)\theta_1+2B_7\left(u_0'u_1'\right)+2B_8\left(u_0u_1\right)=0 \tag{16}$$

The above coupled equations are subjected to the conditions:

$$\begin{aligned}&\text{at}\, y=0: u_0=0,\ u_1=0,\ \theta_0=0 \text{ and } \theta_1=0\\ &\text{at}\, y=1: u_0=0,\ u_1=0,\ \theta_0=1 \text{ and } \theta_1=0.\end{aligned} \tag{17}$$

Here, $B_1=\left(A_1/A_2\right)\left(1+\left(k_1/A_1\right)\right)$; $B_2=\left(A_6/A_2\right)Gr$; $B_3=-\left(A_5/A_2\right)M^2$; $B_4=H^2/A_2$; $B_5=B_3-iH^2$; $B_6=\left(1/\Pr\right)\left(\left(A_4/A_3\right)+\left(\left(4Rd\right)/\left(3A_3\right)\right)\right)$; $B_7=\left(B_1A_2/A_3\right)\left(Ec\right)$; $B_8=\left(A_5/A_3\right)\left(Ec\right)\left(M^2\right)$; $B_9=B_5-B_3$; $B_{10}=Q/A_3$.

The coupled equations from (13) to (16) are solved along with the conditions given in Eq. (17), numerically.

RESULTS AND DISCUSSION

By assigning the numerical values to various parameters, for the physical insight of the problem, velocity (u), temperature *(θ)* and Nusselt number (*Nu*) distributions, for blood – Al_2O_3 were discussed. The obtained results of the investigation are depicted graphically and in tabular form. While performing the simulations against one parameter, the values of other parameters are taken as follows: $t=\pi/4$; $\varepsilon=0.01$; $k_1=3$; $\phi=0.05$; $Q=1$; $Pr=21$; $Ec=1$; $Gr=4$; $M=2$; $Rd=2$; $m=3$ and $H=2$. Also, the thermophysical properties of blood and Al_2O_3 are $\rho_f=1050$, $\rho_n=3970$, $(c_p)_f=3617$, $(c_p)_n=765$, $\kappa_f=0.52$, $\kappa_n=40$, $\sigma_f=0.8$, $\sigma_n=1\times10^{-10}$, $\beta_f=1.8\times10^{-6}$, $\beta_n=8.5\times10^{-6}$ [22, 26].

In order to validate the present numerical work, the results were compared with those reported by Kumar and Srinivas [22] by considering $Gr=R=Ec=0$. This comparison (see Fig. 2) shows that there is an excellent agreement between present numerical work and previously published results.

The velocity profiles against various parameters are shown in Figure 3. Fig. 3(a) illustrates the effect of *H* on the velocity of the fluid. It reveals that a rise in the frequency parameter enhances the velocity of the fluid. As non-Newtonian parameter, *k₁* and the inertial force are related directly; by raising *k₁* the inertial forces reduce the fluid velocity as depicted in Fig. 3(b). The influence of Grashof number *Gr* on u is illustrated in Fig. 3(c). The relation between *Gr* and the velocity describes that the rise in *Gr* decreases the viscosity. This decrease in viscosity aids in the raise of buoyancy forces, and as a consequence, there is a growth in the velocity.

From Fig. 3(d), a fall in the velocity profiles can be noticed with an increase in *M.* This decrement is caused due to the Lorentz force which is a resistive force that results in lowering the velocity.

Figures 3(e) and 4(c) demonstrate the effect of varying thermal radiation (*Rd*) on the fluid velocity and temperature within the channel. The figures reveal that both the velocity and temperature within the channel raises with an increment of *Rd*. This rise in the temperature distribution maybe because of the decrease in thermal conduction of the fluid, which is causing a rise in the heat flux to the fluid. This change in the heat flux results in the rise of the fluid temperature, which enhances the kinetic energy of the fluid, thereby causing a faster flow of the fluid (Fig. 3(e)).

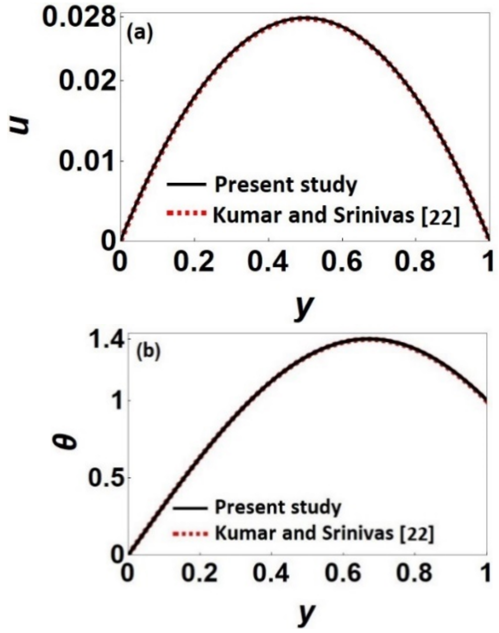

Figure 2. Comparison of (a) Velocity, u and (b) Temperature, θ with the previous work.

Fig. 4(a) depicts the variation of Ec on the temperature distribution. Because of the viscous dissipation, an increase in the Eckert number generates the internal energy, and it reflects in the enhancement of the fluid temperature. The same can be observed from Fig. 4(a) that raising Ec enhances the temperature. From Fig. 4(b), it is clear that as increasing heat source cause the higher temperature. Fig. 4(d) is plotted for temperature distribution, to see the effect of ϕ The addition of nanoparticles into base fluids raises the thermal conductivity. Additional factors such as the size and shape of the particles may also bring changes in the thermal conductivity. Consequently, there is an increase in the temperature distribution as ϕ increases (see Fig. 4(d)).

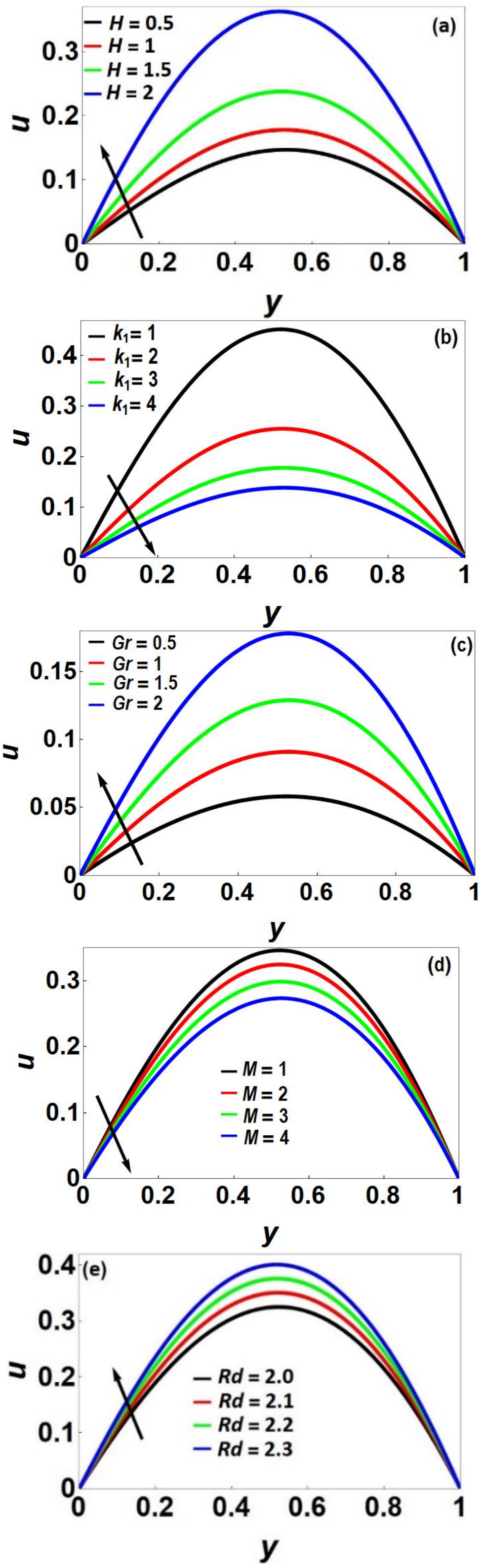

Figure 3. (a) Influence of *H*; (b) Influence of k_1 ; (c) Influence of Gr ; (d) Influence of M ; (e) Influence of Rd on u .

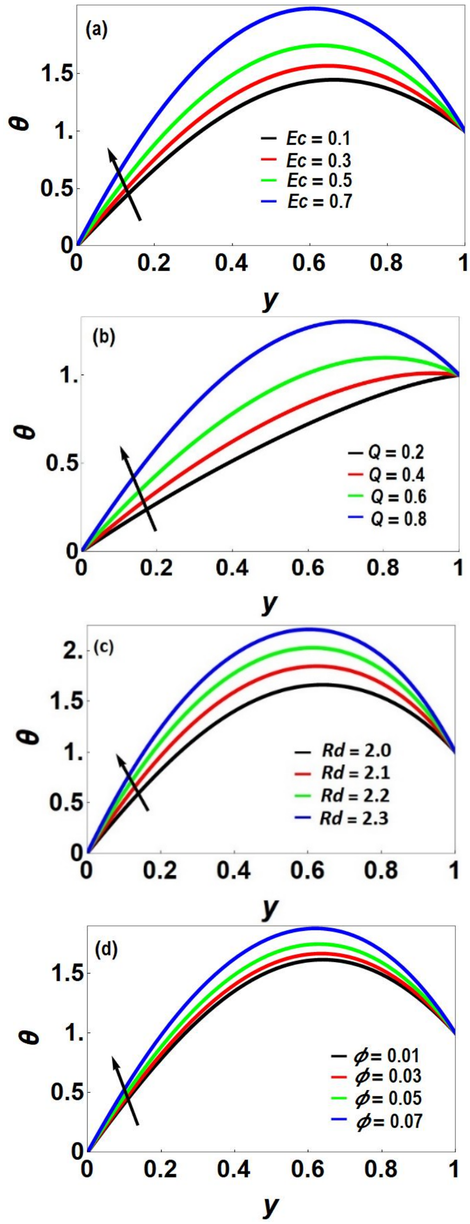

Figure 4. (a) Influence of *Ec;* (b) Influence of Q ; (c) Influence of *Rd;* (d) Influence of ϕ on θ.

From Fig. 5 it is evident that unsteady velocity and unsteady temperature oscillate with increasing time, because the flow of the fluid is driven by an oscillatory pressure gradient. Consequently, u_1 and θ_1 significantly vary with time. Fig. 5(b) illustrates that maximum temperature is drifted towards the boundary layers near channel walls.

The values of Nusselt number (on left and right walls) can be determined as follows [18]:

$$Nu_{0,1} = \frac{h\kappa_{nf}}{\kappa_f\left(T_1 - T_0\right)}\left(\frac{\partial \hat{T}}{\partial \hat{y}}\right) = A_4\left(\frac{\partial \theta}{\partial y}\right)_{y=0,1}. \qquad (18)$$

Table 1. The values of shape factor for various shapes of nanoparticles [6, 27]

Name of the shape	Shape of the nanoparticle	Shape factor (*m*)
Spherical		3
Brick	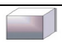	3.7
Cylinder		4.9
Platelet	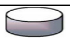	5.7

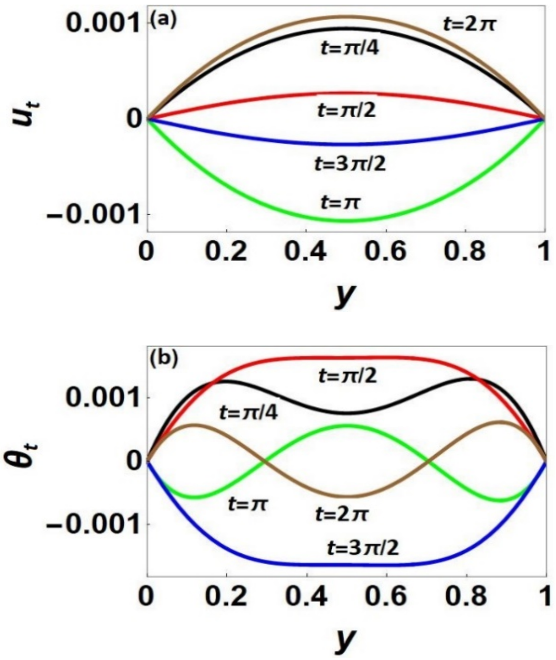

Figure 5. Influence of t on (a) u_t (b) θ_t.

Shape factors values for nanoparticles, used in our calculations, are depicted in Table 1. Table 2 shows the computed values of *Nu* on channel walls for different parameters. Our calculations reveal that heat transfer rate raises on the left wall, $y = 0$ while it drops at the right wall of the channel for increasing values of Gr, ϕ and $Q,$ whereas the Nusselt number decreases with increasing k_1, *M* and *Rd*. This is because a raise in rheological parameter and Hartmann number reduces the fluid velocity near y = 0. Furthermore, the heat transfer rate increases as the particle shape factor increases for any given parameter. One can observe that the heat transfer rate is maximum for the case of platelets like cylindrical, brick and spherically shaped nanoparticles.

Table 2.: Variation of Nu for different values of *Gr*, k_1, *M*, ϕ and *Q*.

Parameter	Value	Shape of Nanoparticle (*m*)							
		Spherical (*m* = 3)		Brick (*m* = 3.7)		Cylinder (*m* = 4.9)		Platelets (*m* = 5.7)	
		$Nu_{y=0}$	$Nu_{y=1}$	$Nu_{y=0}$	$Nu_{y=1}$	$Nu_{y=0}$	$Nu_{y=1}$	$Nu_{y=0}$	$Nu_{y=1}$
Gr	0.5	3.9808	-2.8623	4.0358	-2.8727	4.1258	-2.8872	4.1830	-2.8946
	1	4.2680	-3.1861	4.3201	-3.1938	4.4053	-3.2040	4.4595	-3.2088
	1.5	4.7590	-3.7369	4.8020	-3.7360	4.8733	-3.7327	4.9191	-3.7294
k_1	1	9.7486	-9.1379	10.351	-9.7284	11.431	-10.768	12.1557	-11.466
	2	6.8263	-5.9910	6.7640	-5.8822	6.6890	-5.7293	6.6551	-5.6446
	3	5.6526	-4.7252	5.6651	-4.6933	5.6912	-4.6443	5.7101	-4.6148
M	2	5.6526	-4.7252	5.6651	-4.6933	5.6912	-4.6443	5.7101	-4.6148
	3	5.5173	-4.5740	5.5332	-4.5456	5.5642	-4.5016	5.5868	-4.4749
	4	5.3376	-4.3756	5.3587	-4.3525	5.3974	-4.3162	5.4243	-4.2939
ϕ	0.01	4.3371	-3.4423	4.3470	-3.4440	4.3634	-3.4468	4.3740	-3.4486
	0.03	4.8934	-3.9747	4.9155	-3.9715	4.9527	-3.9659	4.9769	-3.9621
	0.05	5.6526	-4.7252	5.6651	-4.6933	5.6912	-4.6443	5.7101	-4.6148
Q	0.4	2.1001	-0.3467	2.1493	-0.3384	2.2295	-0.3234	2.2810	-0.3127
	0.6	2.7223	-1.2193	2.7753	-1.2202	2.8627	-1.2197	2.9186	-1.2180
	0.8	3.7215	-2.4894	3.7733	-2.4934	3.8583	-2.4976	3.9125	-2.4989
Rd	2	5.6526	-4.7252	5.6651	-4.6933	5.6912	-4.6443	5.7110	-4.6148
	3	3.1298	-1.7740	3.1933	-1.7907	3.2980	-1.8162	3.3648	-1.8312
	4	2.4304	-0.8579	2.4898	-0.8670	2.5881	-0.8809	2.6513	-0.8890

CONCLUSIONS

The hydromagnetic flow of a Powell-Eyring nanofluid with the oscillatory pressure gradient trough the vertical channel was investigated, accounting for the effects of thermal radiation and Joule's heating. This study is helpful in describing the thermal characteristics of the blood flow in the circulatory system. The Shooting technique along with the 4th order R-K method is employed to solve the transformed flow equations. Our analysis indicates that the Joule's heating and thermal radiation affect the flow. An increase in Grashof number and frequency parameter enhances the velocity, whereas the velocity decreases as increasing the intensity of the magnetic field and non-Newtonian parameter. The fluid temperature raises for the higher values of the Eckert number, heat source parameter, radiation parameter, and nanoparticle volume fraction. The unsteady velocity of the fluid and unsteady temperature oscillate with time due to the impact of periodic pressure gradient. From the calculated results, we observed that by increasing the rheological parameter of the base fluid and the intensity of the magnetic field, the heat transfer rate weakens at the left wall. Further, highest rate of heat transfer occurs for the case of platelets (m = 5.7). The hydrodynamic case of the nanofluid flow with a pulsating pressure gradient can be captured by choosing $M = 0$ and $k_1 = 0$

REFERENCES

1. S. S. Suri, H. Fenniri, B. Singh, *J. Occupat. Med. Toxicol.*, **2**(1), 1 (2007).
2. S. U. S. Choi, J. A. Eastman, *ASME Int. Mech. Eng. Cong. Expos.*, **66**, 99 (1995).
3. M. Hatami, J. Hatami, D. D. Ganji, *Comput. Methods, Programs, Biomedicine*, **113**(2), 632 (2014).
4. Y. Menni, A. J. Chamkha, A. Azzi, *Special. Top. Rev. Porous Media Int. J.*, **9**(4), 1 (2018).
5. J. Raza, A. M. Rohni, Z. Omar, *Int. J. Heat Mass Transfer*, **103**, 336 (2016).
6. M. Sheikholeslami, M. Hatami, D. D. Ganji, *Powder Technol.*, **246**, 327 (2013).
7. A. Vijayalakshmi, S. Srinivas, *J. Mech.*, **33**(2), 213 (2017).
8. K. V. Wong, O. De Leon, *Adv. Mechanical Eng.*, **2**, 519659 (2010).
9. F. G. Fowkes, G. D. Lowe, A. Rumley, S. E. Lennie, F. B. Smith, P. T. Donnan, *European Heart J.*, **14**(5), 597 (1993).
10. I. A. Mirza, M. Abdulhameed, S. Shafie, *Appl. Math. Mech.*, **38**(3), 379 (2017).
11. M. M. Molla, M. C. Paul, *Med. Eng. Phys.*, **34**(8), 1079 (2012).
12. G. B. Thurston, N. M. Henderson, M. Jeng, Adv. Hemodynamics Hemorheol., T. V. How (ed.), Jai Press Inc, 2004.
13. M. Y. Abou-zeid, S. S. El-zahrani, H. M. Mansour, *J. Nucl. Part. Phys.*, **4**(3), 100, (2014).
14. S. Jafarzadeh, A. N. Sadr, E. Kaffash, S. Goudarzid, E. Golabe, A. Karimipourf, *Comput. Methods Programs Biomedicine*, **195**, 105545 (2020).
15. P. B. Kumar, S. Srinivas, *Eur. Phys. J. Special. Top.*, **230**, 1465 (2021).
16. W. Chang, G. Pu-Zhen, T. Si-Chao, X. Chao, *Prog. Nucl. Energy*, **58**, 45 (2012).
17. C. K. Kumar, S. Srinivas, A. S. Reddy, *J. Mech.*, **36**(4), 535 (2020).
18. G. Radhakrishnamacharya, M. K. Maiti, *Int. J. Heat Mass Transfer*, **20**(2), 171 (1977).

19. H. M. Shawky, *Heat Mass Transfer*, **45**(10), 1261 (2009).
20. S. Srinivas, C. K. Kumar, A. S. Reddy, *Nonlinear Anal. Model. Control*, **23**(2), 213 (2018).
21. R. K. Selvi, R. Muthuraj, *Ain Shams Eng. J.*, **9**(4), 2503 (2018).
22. P. B. Kumar, S. Srinivas, *Mater. Today, Proc.*, **9**, 320 (2019).
23. S. B. Islami, B. Dastvareh, R. Gharraei, *Int. J. Heat Mass Transfer*, **78**, 917 (2014).
24. M. Sheikholeslami, T. Hayat, A. Alsaedi, *Int. J. Heat Mass Transfer*, **96**, 513 (2016).
25. S. O. Adesanya, J. A. Falade, O. D. Makinde, *Sci. Bull., Politeh. Univ. Buchar., Ser. D,* **77**(1), 25 (2015).
26. M. R. Eid, A. F. Al-Hossainy, M. S. Zoromba, *Commun. Theor. Phys.*, **71**(12), 1425 (2019).
27. N. S. Akbar, A. W. Butt, D. Tripathi, *Results Phys.*, **7**, 2477 (2017).
28. M. Sheikholeslami, M. Sadoughi, *Int. J. Heat Mass Transfer*, **113**, 106 (2017).